Joint modeling of received power, mean delay, and delay spread for wideband radio channels

Ayush Bharti, Ramoni Adeogun, Xuesong Cai, Wei Fan, Francois-Xavier Briol, Laurent Clavier, Troels Pedersen

Joint Modeling of Received Power, Mean Delay, and Delay Spread for Wideband Radio Channels

Ayush Bharti, *Member, IEEE*, Ramoni Adeogun, *Senior Member, IEEE*, Xuesong Cai, Wei Fan, *Senior Member, IEEE*, François-Xavier Briol, Laurent Clavier, *Senior Member, IEEE*, and Troels Pedersen, *Member, IEEE*

***Abstract*— We propose a multivariate log-normal distribution to jointly model received power, mean delay, and root mean square (rms) delay spread of wideband radio channels, referred to as the standardized temporal moments. The model is validated using experimental data collected from five different measurement campaigns (four indoor scenarios and one outdoor scenario). We observe that the received power, the mean delay, and the rms delay spread are correlated random variables, and therefore, should be simulated jointly. Joint models are able to capture the structure of the underlying process, unlike the independent models considered in the literature. The proposed model of the multivariate log-normal distribution is found to be a good fit for a large number of wideband data sets.**

***Index Terms*— Mean delay, millimeter-wave, multivariate log-normal, root mean square (rms) delay spread, temporal moments, wideband radio channels.**

I. Introduction

STANDARDIZED temporal moments, such as received power, mean delay, and root mean square (rms) delay spread, are widely used to summarize power-delay profiles (PDPs) of wideband radio channels. Characterization of these temporal moments is imperative for understanding the effects of multipath propagation on the received signal [1], and hence, for the design and analysis of communication and localization systems. The standardized temporal moments are derived from transformations of the raw temporal moments of the instantaneous power of the received signal. Therefore, the raw moments, and consequently the standardized moments, are dependent random variables. The raw temporal moments have recently been used to estimate parameters of stochastic radio channel models from measurements [2]–[7]. Mean delay and rms delay spread have also been used to fit an extension of the WINNER II model to measurements [8]. In applications where multiple temporal moments are used, it can be valuable to consider their dependences to avoid biases that can occur due to false assumptions of independence.

Independent modeling of received power, mean delay, and rms delay spread is prevalent in the literature, with their empirical averages and cumulative distribution functions (CDFs) being reported frequently while disregarding their dependences. A survey of the empirical data available for the delay properties of indoor radio channel is given in [9], where a variety of marginal models is fit to the mean delay and rms delay spread from the various data sets. They obtained log-normal, Gaussian, and Weibull as the best fit models. The empirical distribution of delay spread has been modeled using a log-normal distribution in the 910 MHz channel [10], [11], the 30–400 MHz frequency band [12], at 460 MHz [13], at 11 GHz [14], and at 39 GHz [15]. A Gaussian distribution for the rms delay spread has also been proposed based on empirical data in [16] and [17]. Recently, the rms delay spread has also been modeled using a bimodal Gaussian mixture distribution [18] and neural networks [19].

The shortcomings of independent modeling become clear by considering jointly the received power and rms delay spread as done in the example in Fig. 1. It is apparent that by fitting independent log-normal models to the received power and the rms delay spread, the marginals of the data are modeled correctly. However, the correlation information in the data is lost on modeling them independently. Delay spread is previously found to be correlated with received power at 60 GHz [20] and to mean delay in the ultrahigh frequency band [21]. One approach to mitigate this problem is to model the standardized moments jointly. An exception to the independent models is the one proposed by Greenstein *et al.* [11] where they accounted for the correlation between rms delay spread and shadow fading after analyzing a wide range of outdoor measurements, mostly in the 900 MHz frequency band. They argued that rms delay spread is log-normally distributed at a given propagation distance, and proposed a joint log-normal model for path gain[1] and delay spread with

Manuscript received May 18, 2020; revised September 22, 2020; accepted December 29, 2020. Date of publication February 24, 2021; date of current version August 4, 2021. This work was supported by the Danish Council for Independent Research performed within the framework of the COST Action CA15104 IRACON under Grant DFF 7017-00265. The work of Ramoni Adeogun was supported by Grant DFF 9041-00146B. The work of François-Xavier Briol was supported by the Lloyds Register Foundation Programme on Data-Centric Engineering at The Alan Turing Institute under EPSRC Grant [EP/N510129/1] *(Corresponding author: Ayush Bharti.)*.

Ayush Bharti, Ramoni Adeogun, Xuesong Cai, Wei Fan, and Troels Pedersen are with the Department of Electronic Systems, Aalborg University, 9220 Aalborg, Denmark (e-mail: ayb@es.aau.dk; ra@es.aau.dk; xuc@es.aau.dk; wfa@es.aau.dk; troels@es.aau.dk).

François-Xavier Briol is with the Department of Statistical Science, University College London, London WC1E 6BT, U.K., and also with the Data-Centric Engineering Programme, The Alan Turing Institute, London NW1 2DB, U.K. (e-mail: f.briol@ucl.ac.uk).

Laurent Clavier is with the IMT Lille Douai, University of Lille, CNRS, UMR 8520, F-59000 Lille, France (e-mail: laurent.clavier@imt-lille-douai.fr).

Color versions of one or more figures in this article are available at https://doi.org/10.1109/TAP.2021.3060099.

Digital Object Identifier 10.1109/TAP.2021.3060099

[1]Greenstein *et al.* [11] defined path gain as the ratio of received power to transmitted power.

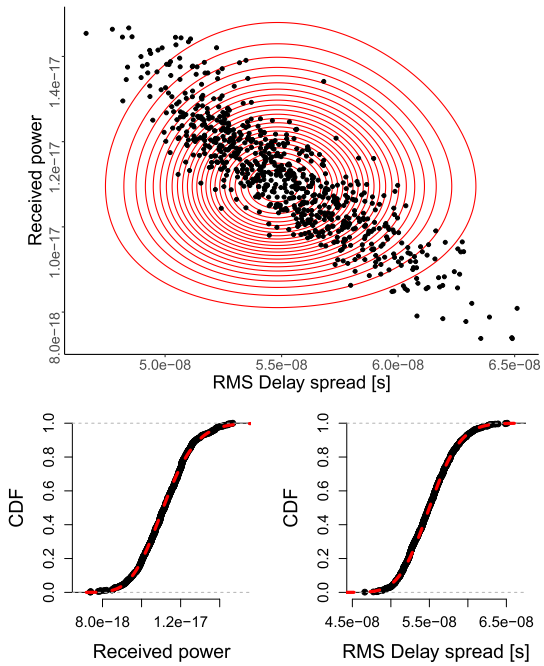

Fig. 1. Scatter plot of received power and rms delay spread obtained from AAU-Hall measurements (see Section IV-D) is shown in black (above). The contour lines from independently fitting log-normal distribution to the measurements are shown in red. The empirical CDFs of the marginals are also shown with the fitted log-normal CDF in red (below). Note that the received power is unitless.

a correlation coefficient of -0.75. However, they did not take mean delay into account. Moreover, the correlation coefficient was based on qualitative analysis of scatter plots and on a single measurement setting. The mutual relations between the means of the raw temporal moments have been modeled in [22]–[24] for the in-room case, while their joint distribution was not studied. To the best of our knowledge, joint characterization of the temporal moments in the millimeter-wave (mm-wave) band has not been done before.

Potentially, the temporal moments could be modeled jointly using a multivariate distribution such that the model could be fitted to new measurements. Joint modeling of multivariate random variables is considerably more involved than modeling of scalar random variables because the model is required to represent the marginals and the dependence structure in the data at the same time. Only a few univariate probability distribution functions (pdf's) exist that have unique multivariate extensions, such as the multivariate Gaussian, log-normal, and Gamma distributions [25]. Copulas [26] can also be used to model the dependence structure between the random variables, especially when the marginal distributions lead to a multivariate distribution that is difficult to handle due to the lack of analytical expression or difficulties to estimate the parameters.

After considering several of these methods, we conclude that the multivariate log-normal is a reasonable choice that provides a good balance between goodness-of-fit and ease of interpretation. Moreover, there is substantial support for log-normality of standardized temporal moments in the literature. In this article, we propose and validate the multivariate log-normal model using a wide variety of measurements taken in different scenarios and frequency ranges, including both indoor and outdoor settings. Measurement campaigns were conducted at Lund University [27], University of Lille [28], and Aalborg University (AAU) [29]. We also present mm-wave measurements from one indoor and one outdoor campaign in the 28–30 GHz band conducted recently at AAU. We compare the proposed model with the multivariate Gaussian and independent marginal models in terms of the Akaike information criterion (AIC). Finally, we investigate the model fits to the raw and standardized temporal moments from the measurements. Preliminary results have been published in the conference publication [30].

This article is organized as follows. Section II describes the raw and standardized temporal moments, and Section III presents the model. In Section IV, we compare the proposed model with other modeling choices. Sections V and VI compare the model fits to the raw and standardized temporal moments of the measurements, respectively. Finally, the conclusions are outlined in Section VII.

II. Temporal Moments

Consider a measurement campaign where the channel transfer function between fixed transmit and receive antennas is recorded using a vector network analyzer (VNA). Sampling the transfer function, $H(f)$, at N_s frequency points in the measurement bandwidth B results in a separation of $\Delta f = B/(N_s - 1)$ between the points. We assume that the measurement noise at the nth frequency point, W_n, is additive and independent of the transfer function, H_n. Then, the measured frequency-domain signal, Y_n, reads

$$Y_n = H_n + W_n, \quad n = 0, 1, \ldots, (N_s - 1). \tag{1}$$

Discrete-frequency, continuous-time inverse Fourier transform gives the $1/\Delta f$-periodic measured time-domain signal

$$y(t) = \frac{1}{N_s} \sum_{n=0}^{N_s-1} Y_n \exp(j2\pi n \Delta f t). \tag{2}$$

Note that $y(t)$ is often referred to as the impulse response despite suffering from limited bandwidth and noise. This terminology is somewhat misleading since strictly speaking the impulse response is the inverse Fourier transform of $H(f)$. For large bandwidth and high signal-to-noise ratio (SNR), $y(t)$ can be used as an approximation to the impulse response in the time interval $[0, 1/\Delta f]$, provided that the impulse response decays rapidly enough. To avoid this confusion, we refer to $y(t)$ as the measured signal.

The raw temporal moments are summary statistics of the measured signal $y(t)$, where the kth temporal moment is defined as

$$m_k = \int_0^{\frac{1}{\Delta f}} t^k |y(t)|^2 \mathrm{d}t, \quad k = 0, 1, \ldots, (K - 1). \tag{3}$$

Here, a total of K raw temporal moments are computed "instantaneously" per realization of $y(t)$, giving the K-dimensional vector $\mathbf{m} = [m_0, m_1, \ldots, m_{K-1}]^\top$. The raw temporal moments are correlated random variables as they are

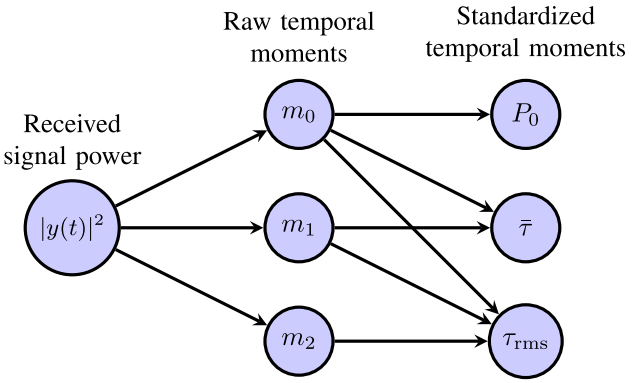

Fig. 2. Connections between the magnitude square received signal and the summary statistics (raw- and standardized temporal moments).

all derived from the received signal power, $|y(t)|^2$. The kth temporal moment is measured in [second]^k.

The standardized temporal moments are obtained from the first three raw temporal moments. The received power, P_0, the mean delay, $\bar{\tau}$, and the rms delay spread, τ_{rms}, are given as

$$P_0 = m_0, \quad \bar{\tau} = \frac{m_1}{m_0}, \quad \text{and} \quad \tau_{\text{rms}} = \sqrt{\frac{m_2}{m_0} - \left(\frac{m_1}{m_0}\right)^2}. \quad (4)$$

The unit of $\bar{\tau}$ and τ_{rms} is in seconds whereas P_0 is unitless. The deterministic relationship between the raw and the standardized temporal moments is depicted in Fig. 2. The nonlinearity of the above transformations and the dependence of the raw temporal moments complicates the joint characterization of mean delay and rms delay spread. Summarizing N_{real} realizations of the measured signal into K temporal moments therefore results in the $K \times N_{\text{real}}$ dimensional matrix, $\mathbf{M} = [\mathbf{m}^{(1)}, \ldots, \mathbf{m}^{(N_{\text{real}})}]$. We will focus our discussion on the first three temporal moments, (m_0, m_1, m_2), as they suffice for the received power, mean delay, and rms delay spread but it is straightforward to extend the framework to include more moments as long as the marginal distributions fit the same distribution.

Note that the standardized temporal moments in (4) are computed from the measured signal, $y(t)$, rather than the channel impulse response. The impulse response is unobservable due to the noise and bandwidth limitations. It is widespread practice to employ a thresholding procedure to reduce the effect of the measurement noise on the estimation of temporal moments. However, such procedures require the setting of a threshold or dynamic range. The choice of the threshold affects the resulting estimates in a manner that makes a comparison between measurements obtained with different equipment difficult. For this reason, we omit any thresholding procedure in the present work.

The finite measurement bandwidth also manifests itself in the rms delay spread as an approximately additive term equal to the delay spread of the transmitted signal. This effect can be partially removed by subtracting the delay spread of the frequency window. This is widespread practice in the literature and results in a good approximation if the bandwidth is large and the SNR is high. However, in the case of low SNR and small-signal bandwidth, this can lead to inaccurate and sometimes negative estimates of the delay spread. For the measurements considered in Section IV, where the bandwidth is very large, the effect of the transmitted signal can be ignored. Hence, we make no attempt to compensate for the effect of a finite measurement bandwidth.

III. Proposed Statistical Model

We intend to jointly model the first three raw temporal moments, (m_0, m_1, m_2), and use the transformation in (4) to simulate the mean delay and rms delay spread. In principle, the standardized temporal moments could be modeled instead of the raw moments. However, the distribution on the raw moments implies a distribution on the standardized moments from which sampling is straightforward. Modeling the raw moments has the added advantage that their means and covariances are easier to compute analytically for a given channel model than those of the standardized moments due to the nonlinear transformation.

We model the vector $\mathbf{m} = [m_0, m_1, m_2]^\top$ as a multivariate log-normal variable. The exponential of a random vector following a multivariate Gaussian distribution is multivariate log-normal distributed. Let $\mathbf{x}$ be a K-variate normal random vector with mean $\boldsymbol{\mu}$ and covariance matrix $\boldsymbol{\Sigma}$. Then its entrywise exponentiation, $\mathbf{m} = \exp(\mathbf{x})$, yields a log-normal vector with pdf

$$f(\mathbf{m}; \boldsymbol{\mu}, \boldsymbol{\Sigma}) = \frac{\prod_{k=0}^{K-1} (m_k)^{-1}}{\sqrt{(2\pi)^K \det \boldsymbol{\Sigma}}} \times \exp\left(-\frac{1}{2}(\ln(\mathbf{m}) - \boldsymbol{\mu})^\top \boldsymbol{\Sigma}^{-1} (\ln(\mathbf{m}) - \boldsymbol{\mu})\right). \quad (5)$$

Here, the logarithm is taken entrywise. By property of the marginals of the multivariate Gaussian, it is easy to see that this transform results in a distribution with log-normal marginals. Note that the parameters of a multivariate log-normal are the mean vector and the covariance matrix of the associated multivariate Gaussian distribution. The entries of $\boldsymbol{\mu}$ and $\boldsymbol{\Sigma}$ are given as $\mu_k = \mathbb{E}[\ln m_k]$ and $\Sigma_{kk'} = \text{cov}(\ln m_k, \ln m_{k'})$, for $k, k' = 0, 1, \ldots, K-1$, respectively. Given that raw temporal moments are log-normally distributed, their means and covariances can be related to μ and Σ as

$$\mathbb{E}[m_k] = \exp\left(\mu_k + \frac{1}{2}\Sigma_{kk}\right), \quad \text{and} \quad (6)$$

$$\text{cov}(m_k, m_{k'}) = \exp\left(\mu_k + \mu_{k'} + \frac{1}{2}(\Sigma_{kk} + \Sigma_{k'k'})\right) \times (\exp(\Sigma_{kk'}) - 1). \quad (7)$$

Note that we model the raw temporal moments as opposed to Greenstein *et al.* [11] who model shadow fading and rms delay spread as jointly log-normal. With the proposed model, log-normality is preserved for the received power and mean delay due to the multiplicative transform applied on m_0 and m_1. However, the distribution of rms delay spread depends on a more complicated transformation (see (4)) and hence cannot easily be derived in closed form.

TABLE I
SUMMARY OF DIFFERENT MEASUREMENT DATA SETS

Data set	Bandwidth (GHz)	No. of samples	No. of realizations	Antenna Tx/Rx	Dimensions (m^3)	Scenario	Environment
Lund Data [27]	58-62	801	625	Biconical/Open waveguide	$3 \times 4 \times 3$	NLOS	Small room
Lille Data [28]	59-61	1601	750	Microstrip/Microstrip	$5.20 \times 7.15 \times 2.90$	LOS	Large room
AAU-Industry [29]	3-8	5001	95	Biconical/Biconical	$33 \times 14 \times 6$	Both	Industry hall
AAU-Hall	28-30	1500	720	Biconical/Biconical	$44 \times 25 \times 10$	NLOS	Large hall
AAU-Outdoor	28-30	2000	360	Horn/Biconical	—	LOS	Outdoor

A. Estimation of Parameters

The parameters of the proposed model need to be estimated from measured data in order to use the model for simulation purposes. Here, we refer to the matrix of raw temporal moments, $\mathbf{M}$, as the data. This data matrix is obtained by summarizing N_{real} realizations of the measured signal using (3). Assuming independent and identically distributed (i.i.d.) realizations, maximum likelihood estimation of $\boldsymbol{\mu}$ and $\boldsymbol{\Sigma}$ is achieved by solving the optimization problem

$$(\hat{\boldsymbol{\mu}}, \hat{\boldsymbol{\Sigma}}) = \underset{\boldsymbol{\mu}, \boldsymbol{\Sigma}}{\operatorname{argmax}} \prod_{i=1}^{N_{\text{real}}} f\left(\mathbf{m}^{(i)}; \boldsymbol{\mu}, \boldsymbol{\Sigma}\right). \tag{8}$$

Since $\boldsymbol{\mu}$ and $\boldsymbol{\Sigma}$ are the mean vector and the covariance matrix, respectively, of the associated multivariate Gaussian distribution, their maximum likelihood estimates, $\hat{\boldsymbol{\mu}}$, and $\hat{\boldsymbol{\Sigma}}$, are

$$\hat{\boldsymbol{\mu}} = \frac{1}{N_{\text{real}}} \sum_{i=1}^{N_{\text{real}}} \ln \mathbf{m}^{(i)}, \quad \text{and} \tag{9}$$

$$\hat{\boldsymbol{\Sigma}} = \frac{1}{N_{\text{real}}} \sum_{i=1}^{N_{\text{real}}} \left(\ln \mathbf{m}^{(i)} - \hat{\boldsymbol{\mu}}\right)\left(\ln \mathbf{m}^{(i)} - \hat{\boldsymbol{\mu}}\right)^{\top}. \tag{10}$$

B. Simulation From the Model

Given a particular value of $\boldsymbol{\mu}$ and $\boldsymbol{\Sigma}$, simulation from the proposed model is straightforward. To generate one sample of $\mathbf{m}$, or subsequently, one sample of $(P_0, \bar{\tau}, \tau_{\text{rms}})$, the following steps should be performed.

1) Draw $\mathbf{x} \sim \mathcal{N}(\boldsymbol{\mu}, \boldsymbol{\Sigma})$.
2) Compute entrywise exponential, $\mathbf{m} = \exp(\mathbf{x})$.
3) Compute $\bar{\tau}$ and τ_{rms} from (4).

IV. MEASUREMENT DATA DESCRIPTION

We now describe the different radio channel measurements used to validate the proposed model. An overview of the measurement data sets is given in Table I. The parameter estimates obtained after fitting the proposed model to the measurements are reported in Table II.

A. Data Set From Lund University

Polarimetric radio channel measurements at 60 GHz was recorded in a small meeting room of dimensions $3 \times 4 \times 3$ m^3 using a VNA [27]. The room consisted of a table, whiteboard, bookshelves, and a window on one of the walls. The receive antenna was placed at one corner of the room and the transmit antenna was placed on the table. A water-filled human phantom was used to block the line-of-sight (LOS) path to emulate non-line-of-sight (NLOS) scenario. A 5×5 virtual array of dual-polarized antennas was used with an interelement spacing of 5 mm at both the transmitter and the receiver. This resulted in a 25×25 dual-polarized MIMO system, however, in this article, we only use the vertical–vertical polarized channels. Measurements were performed in the bandwidth range of 58–62 GHz using 801 equally spaced frequency points. For further details on the measurement campaign, see [27].

B. Data Set From Lille University

Measurements were taken in a computer laboratory of floor area 7.15×5.2 m^2 at 26 sites, covering the whole room. The 60 GHz channel sounder developed at IEMN [28] used two heterodyne emission and reception heads developed by monolithic integration with frequencies ranging from 57 to 59 GHz and with intermediate frequencies of 1 to 3 GHz. A dedicated network analyzer allows, after calibration, the vectored measure of the frequency transfer function by steps of 1.25 MHz. The resulting impulse response has a delay resolution of 0.5 ns and a maximum measurable delay of 800 ns. In this article, we select a subset of the entire data set, specifically, taking the measurements from the first three sites having the same distance between the transmit and receive antennas in LOS condition. Each site consists of 250 positions separated by 2 mm. The transmitter was fixed in a corner, close to the roof, pointed toward the opposite corner. The receiver was oriented toward the transmitter in the horizontal plane but not in the vertical one. Horizontal linear polarization patch antennas were employed.

C. AAU Data, Industry Scenario

Short-range ultrawideband measurement campaigns were conducted in a $33 \times 14 \times 6$ m^3 industrial factory hall at the Smart Production Lab, AAU. The factory hall was a typical high clutter density environment with large metallic machinery such as welding machines, hydraulic press, and material processing machines. Measurements were collected over the frequency range 3–8 GHz using a Rhode & Schwarz ZND 8.5 GHz VNA and omnidirectional broadband biconical antennas at both the transmitter and the receiver. During the measurements, the transmitter was placed at a fixed location and the receiver location was varied to obtain horizontal distances between 1 and 9 m. A total of 95 channel transfer functions were obtained with a frequency resolution of 1 MHz

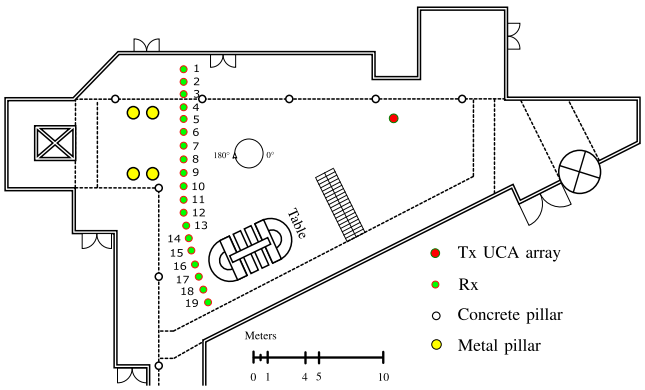

(a)

(b)

Fig. 3. (a) Layout and (b) photograph of the indoor hall taken during the measurement campaign conducted at Aalborg University. The measurements corresponding to the first receive antenna array position are presented in this article.

corresponding to 5001 samples over the 5 GHz bandwidth. Detailed description of the measurements can be found in [29].

D. AAU Data, Hall Scenario

Measurements were conducted in a large hall scenario as illustrated in Fig. 3(a). A photograph taken during the measurement campaign is also shown in Fig. 3(b). The hall had a floor area of 44×25 m^2 with a height of approximately 10 m. As shown in the picture and the layout sketch, tables, metallic pillars, concrete pillars, stairs, etc. were in the hall. The VNA measurements were taken with the ultrawideband radio-over-fiber channel sounder developed at AAU [31]. Quasi-omnidirectional biconical antennas [32] were used. The receive antenna was fixed with a height of 1 m to the ground while transmit antenna was installed on a rotator and rotated with 720 uniform steps on a circle with a radius of 0.54 m. In each step, the channel transfer function from 28 to 30 GHz was swept with 1500 samples in the frequency domain. In this article, we analyze the first of the 19 different locations recorded. For this location, the transmitter-receiver distance was around 15 m in NLOS condition.

E. AAU Data, Outdoor Scenario

Outdoor measurements were conducted in an open area in-between the two buildings as shown in Fig. 4. The same

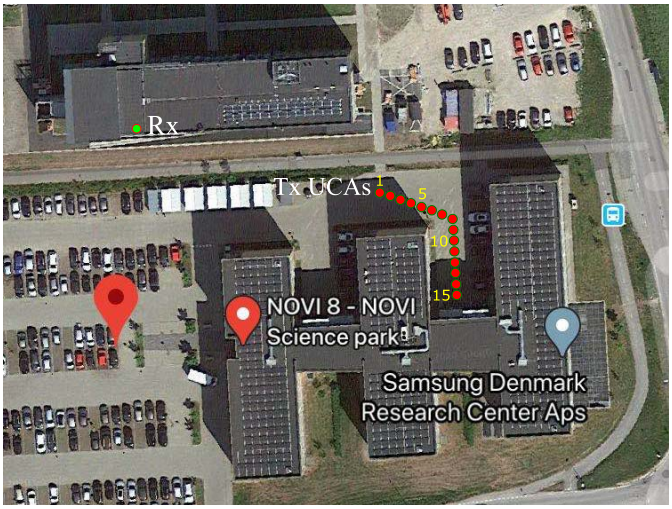

(a)

(b)

Fig. 4. (a) Aerial view and (b) photograph of the environment for the outdoor measurement campaign conducted at Aalborg University. Measurements from transmit antenna location number 7 are presented in this article.

channel sounder is used as in the indoor hall scenario. In this case, the transmitter antenna was rotated with a radius of 0.25 m in 360 uniform steps. In each step, the channel transfer function from 28 to 30 GHz was swept with 2000 samples. The receive antenna was fixed on a roof edge with a height of around 20 m. To increase the SNR, the receive antenna was replaced by a horn antenna with half-power-beamwidths around 30° in both azimuth and elevation. Moreover, its main beam was down tilted to appropriately cover the transmit antenna. Data were collected from 15 transmit transmit antenna locations as indicated in Fig. 4. The data presented in this article are from the seventh location which was in LOS condition.

V. Model Comparison

To characterize the raw temporal moments jointly, their marginal distributions as well as their correlation structure needs to be well represented. We compare the proposed model against competing model choices for the available data sets.

TABLE II

PARAMETER ESTIMATES OBTAINED USING MAXIMUM LIKELIHOOD ESTIMATION. EACH ENTRY CORRESPONDS TO THE ESTIMATE FOR SOME SCALAR PARAMETER θ, WHICH CORRESPONDS TO AN ELEMENT OF EITHER THE 3-D MEAN (COLUMN) VECTOR $\boldsymbol{\mu}$ OR THE 3×3 DIMENSIONAL COVARIANCE MATRIX $\boldsymbol{\Sigma}$. THE NUMBER IN BRACKET (δ) IS THE HALF-WIDTH OF THE 95% CONFIDENCE INTERVAL FOR THAT PARAMETER, SO THAT THE INTERVAL TAKES THE FORM $(\theta - \delta, \theta + \delta)$

Data set	Mean vector $\hat{\boldsymbol{\mu}}(\pm\delta)$	Upper triangle of Covariance matrix $\hat{\boldsymbol{\Sigma}}(\pm\delta)$		
Lund	–39 (4×10^{-3}) –57 (4×10^{-3}) –74 (6×10^{-3})	2.8 $(0.3)\times10^{-3}$	2.5 $(0.3)\times10^{-3}$ 2.6 $(0.3)\times10^{-3}$	1.4 $(0.3)\times10^{-3}$ 2.1 $(0.3)\times10^{-3}$ 5.3 $(0.6)\times10^{-3}$
Lille	–29 (0.03) –47 (0.03) –63 (0.06)	0.19 (0.02)	0.15 (0.02) 0.14 (0.01)	0.11 (0.03) 0.19 (0.03) 0.70 (0.07)
AAU-Industry	–36 (0.31) –53 (0.18) –70 (0.18)	2.34 (0.67)	1.36 (0.40) 0.82 (0.23)	1.24 (0.38) 0.77 (0.23) 0.84 (0.24)
AAU-Hall	–39 (9×10^{-3}) –56 (7×10^{-3}) –72 (5×10^{-3})	1.4 $(0.14)\times10^{-2}$	1.2 $(0.12)\times10^{-2}$ 1.0 $(0.11)\times10^{-2}$	6.6 $(0.76)\times10^{-3}$ 6.2 $(0.68)\times10^{-3}$ 4.6 $(0.48)\times10^{-3}$
AAU-Outdoor	–40 (1.2×10^{-2}) –56 (9×10^{-3}) –71 (5×10^{-3})	1.3 $(0.20)\times10^{-2}$	9.9 $(0.14)\times10^{-3}$ 7.6 $(1.1)\times10^{-3}$	5.2 $(0.82)\times10^{-3}$ 4.2 $(0.64)\times10^{-3}$ 2.7 $(0.40)\times10^{-3}$

TABLE III

AIC VALUES FOR DIFFERENT MODEL CHOICES FOR THE RAW TEMPORAL MOMENTS. BEST MODEL IS INDICATED IN BOLD. NOTE THAT THE JOINT AIC FOR THE INDEPENDENT MODELS IS THE SUM OF THE AIC VALUES OF THE THREE MARGINALS

Data set	Multivariate Log-normal	Multivariate Gaussian	Independent Log-normal marginals	Independent Gaussian marginals	Independent Gamma marginals
Lund	**–219636.0**	–219573.9	–217787.6	–217750.2	–217777.0
Lille	–208357.2	**–208665.6**	–205657.4	–204816.6	–205589.4
AAU-Industry	**–29815.61**	–28922.53	–29337.3	–28604.83	–29201.75
AAU-Hall	**–247225.8**	–247212.2	–243329.2	–243348.8	–243342.9
AAU-Outdoor	–125244.8	**–125286.7**	–122385.1	–122342.4	–122374.1

A. Model Comparison Using AIC

We compare the proposed joint model with the model of a multivariate Gaussian distribution. We also include three independent models for the raw temporal moments based on log-normal, Gaussian, and Gamma distributions. We omit comparison with the multivariate Gamma distributions in [25] as they did not give useful results when fitted to the raw temporal moments. Model comparison is done by computing the AIC value [33] of the competing models. AIC is a common tool for model selection that estimates the quality of different models relative to each other. It compares models through their likelihoods, but penalizes models with a larger number of parameters κ. One motivation for this penalty comes from Ockham's razor, which states that, when comparing models, one should prefer the simplest model which explains the data well. The criterion is computed as follows:

$$\mathrm{AIC} = -2\mathcal{L} + 2\kappa \tag{11}$$

where $\mathcal{L}$ is the maximized log-likelihood of the data. Given a set of models fitted by maximum likelihood to the same data, the preferred model is the one with the lowest AIC value. The reader is referred to [34, Ch. 2] for a detailed discussion. We also considered the Bayesian information criterion (BIC), which penalizes more than AIC for a large number of parameters (see [34, Ch. 3] and [35]). However, the ordering of the models was found to be the same for both the criteria, and therefore we omit the BIC values here.

The models are fitted to the five aforementioned data sets by maximizing their likelihood. The parameter estimates obtained for the proposed model are reported in Table II. The AIC values of the joint fit of the raw temporal moments are reported in Table III, with $\kappa = 9$ for the multivariate distributions, and $\kappa = 6$ for the independent marginal models. The proposed model comes out as the better choice for the joint fit for three out of five data sets, with the multivariate Gaussian performing better for Lille Data and AAU-Outdoor. However, the AIC values for both the joint models are close to each other. It is evident that modeling the random variables independently leads to a significantly poorer fit than either of the joint models, no matter which distribution is chosen. We remark that using more complicated models such as copulas [26] to model the dependence structure may lead to a better fit, but could be harder to interpret.

B. Log-Normal Versus Gaussian Marginals

We now compare the marginal fits of the multivariate log-normal and Gaussian distributions for modeling the raw temporal moments. To assess model fit, the quantiles of the data are plotted against the theoretical quantiles of the model being assessed. If the model is a good fit, then the quantiles of the data and the theoretical quantiles should be close to

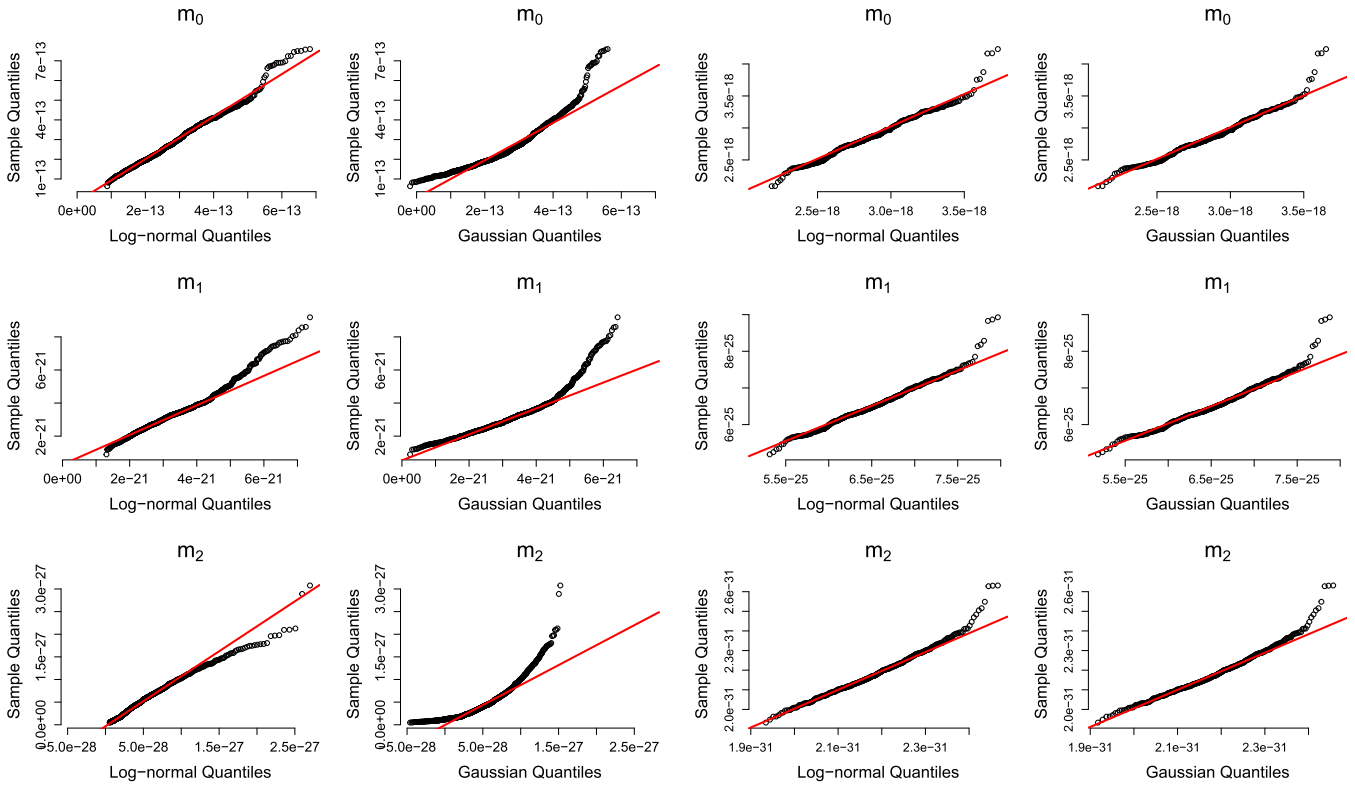

Fig. 5. Quantiles of the measured raw temporal moments from Lille (left) and AAU-Outdoor (right) data versus the theoretical quantiles of fitted log-normal and Gaussian distributions. The theoretical quantile-quantile line passing through the first and third quantile is shown in red.

one another, and the points will hence lie approximately on a straight line. On the other hand, any deviation from this line might indicate issues with the fit of the model. See [36, Sec. 10.2] for more details. We show the Q-Q plots for two of the five data sets, namely the Lille and the AAU-Outdoor data, in Fig. 5, as they highlight the difference between the fits obtained from both the distributions. The Q-Q plots of AAU-Outdoor data are representative of what we observed for the other data sets, therefore we exclude reporting them.

We observe that for AAU-Outdoor data, the marginals are well-modeled by both the log-normal and the Gaussian distributions. The fit is similar for both distributions, and it is not apparent which model performs better. As can be seen in Fig. 6, the marginals in AAU-outdoor data are very close to being symmetric, which means that the Gaussian fits well. However, for the Lille data, it is evident that the log-normal distribution outperforms the Gaussian in terms of the marginals. The log-normal is able to model the left tail and the center of the distribution very well, but sometimes performs poorly for the right tail. On the other hand, the Gaussian is not able to model either of the tails. Moreover, the Gaussian assigns non-zero probabilities to quantiles below zero, which is not the case for the data as temporal moments are non-negative random variables. Hence, the multivariate log-normal is a better choice. Note that a good marginal fit does not imply good overall fit in terms of AIC and vice-versa, as is the case for Lille data. This is simply because the AIC measures a different property of the model which does not require the marginals to fit perfectly.

The deviation of the right tail of the data from the fitted marginals is to be expected due to the low number of such extreme points. Such points are in-frequent and could potentially arise due to a number of factors such as noise, interference, measurement conditions, etc. Therefore, we argue that the right tail is not as important to model perfectly, and thus make no adjustment for it. However, this should be scrutinized further in applications where this effect could be important.

VI. Model Fit to Raw Temporal Moments

The parameter estimates, obtained by fitting the proposed model to the data sets using (9) and (10), are reported in Table II. We also compute and report the 95% confidence intervals for each of the estimates in Table II (see Appendix for details). The confidence intervals are very small for the mean estimates, and an order of magnitude smaller for the covariance estimates. The fit of the proposed model to the various data sets is shown in Fig. 6 where each row corresponds to a particular data set. The marginal distributions of the data and the fitted model are shown on the left while 2-D scatter plots for all pairs of temporal moments are shown on the right along with contour lines of the fitted distribution.

First, we observe in Fig. 6 that the distribution of the raw temporal moments varies across the different data sets. This is attributed to the contrasting scenarios that the measurements were taken in, along with the use of different equipment, antennas, and measurement settings. We also observe that the raw temporal moments are highly correlated random variables.

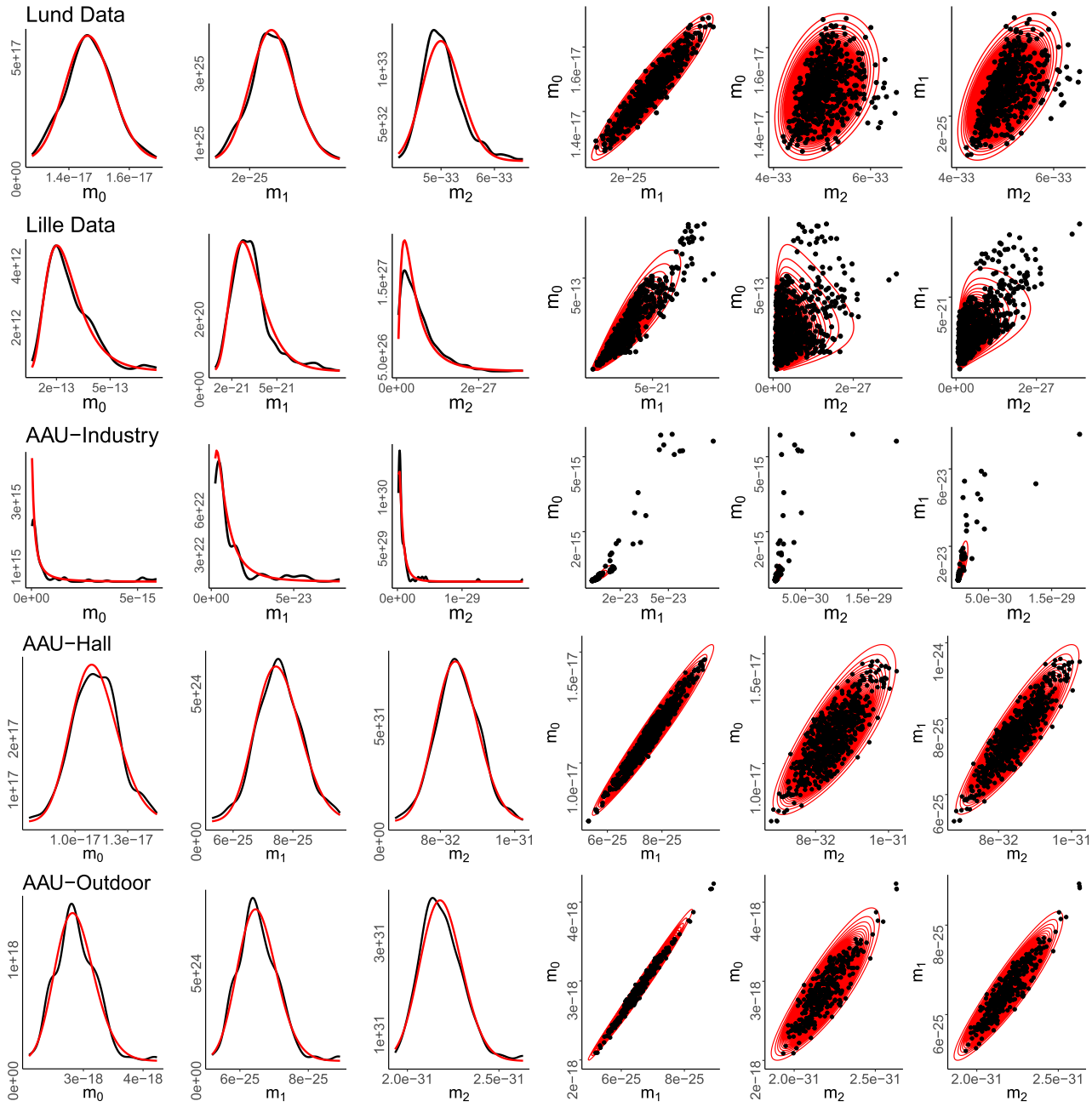

Fig. 6. Density estimates and scatter plots of raw temporal moments obtained from the different measurements (shown in black) versus the density and contour plots of the fitted proposed model (shown in red). Each row corresponds to one of the data sets. All the axes are in linear scale. The parameter estimates are in Table II.

Marginal distributions for Lille and AAU-Industry data are skewed, while those from other data sets are more symmetric. We notice a fanning out of the scatter plots on the top-right of all the indoor data sets, which is not present in the outdoor data. Despite the variability in the data, the proposed model fits the data well, even the skewed ones. There is a high correlation between the raw moments, in particular between m_0 and m_1, since the basic functions used to compute them in (3) are not orthogonal. This is captured well by the model.

VII. Model Fit to Standardized Moments

We now compare the distribution of the standardized temporal moments obtained from the measurements with those from the proposed model. Mean delay and rms delay spread are computed from the raw temporal moments using (4), while the received power is equal to m_0. Pairwise scatter plots of P_0, $\bar{\tau}$, and τ_{rms} from the data and the proposed joint model are shown in Fig. 7. We also include the samples obtained from independently fitting a log-normal distribution to the standardized moments from the data sets. The log-normal is chosen as it was the best in terms of AIC amongst the independent models as per Table III. Here, we exclude the AAU-Industry data as the low number of sample points makes it difficult to make any useful conclusions on the correlation behavior. We observe in Fig. 7 that the standardized temporal moments are also dependent

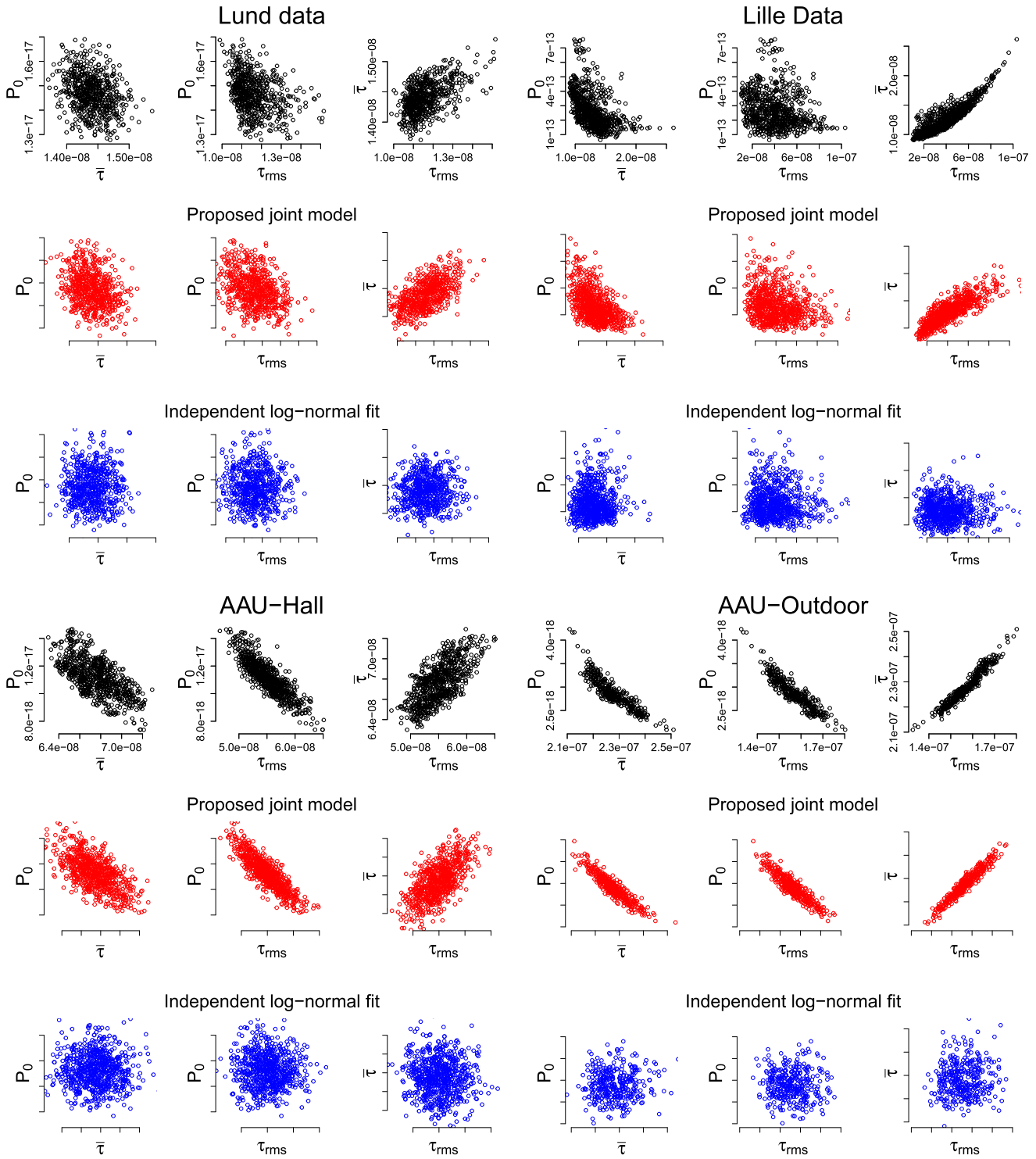

Fig. 7. Scatter plots of received power, mean delay, and rms delay spread from data (in black), and from the proposed model (in red). The samples simulated by independently fitting log-normal marginals to P_0, $\bar{\tau}$, and τ_{rms} from the data are in blue. Number of points simulated is same as in the measurements. The scales of the corresponding plots are the same.

random variables, and the proposed model is able to capture their dependence structure. In contrast, correlation information between the variables is lost when they are simulated independently.

Sample Pearson correlation coefficients between P_0, $\bar{\tau}$, and τ_{rms} from the data are given in Table IV. For paired samples $\{(a_1, b_1), \ldots, (a_m, b_m)\}$, the sample Pearson correlation coefficient is defined as

$$\hat{\rho}_{a,b} = \frac{\sum_{j=1}^{m}(a_j - \bar{a})(b_j - \bar{b})}{\sqrt{\sum_{j=1}^{m}(a_j - \bar{a})^2}\sqrt{\sum_{j=1}^{m}(b_j - \bar{b})^2}} \tag{12}$$

where $\bar{a}$ and $\bar{b}$ are the sample means. We also compute 95% confidence intervals for the correlation estimates using the

TABLE IV

SAMPLE PEARSON CORRELATION COEFFICIENTS BETWEEN STANDARDIZED TEMPORAL MOMENTS OF MEASURED DATA. THE CORRELATION COEFFICIENTS FOR THE MODEL IS COMPUTED USING 10 000 SAMPLES OF SIMULATED DATA. THE NUMBER IN PARENTHESIS (ϵ) IS THE 95% BOOTSTRAP CONFIDENCE INTERVAL OF THE CORRELATION ESTIMATES COMPUTED USING 1000 RESAMPLES, SUCH THAT THE INTERVAL IS OF THE FORM $(\rho - \epsilon, \rho + \epsilon)$

Data set	$\hat{\rho}_{P_0,\bar{\tau}}$		$\hat{\rho}_{P_0,\tau_{\text{rms}}}$		$\hat{\rho}_{\bar{\tau},\tau_{\text{rms}}}$	
	Data	**Model**	**Data**	**Model**	**Data**	**Model**
Lund	–0.28 (± 0.06)	–0.28	–0.35 (±0.05)	–0.36	0.53 (±0.05)	0.52
Lille	–0.48 (±0.03)	–0.51	–0.20 (±0.05)	–0.19	0.89 (±0.02)	0.83
AAU-Hall	–0.66 (±0.03)	–0.65	–0.87 (±0.02)	–0.87	0.70 (±0.03)	0.70
AAU-Outdoor	–0.91 (±0.01)	–0.92	–0.93 (±0.01)	–0.93	0.97 (±0.004)	0.97

bootstrap method [37, Ch. 6]. The correlation coefficients obtained from the fitted model, computed from 10 000 samples to get a robust estimate, are also reported in Table IV. Mean delay and rms delay spread have a positive correlation that varies from 0.53 for the Lund data to as high as 0.97 for AAU-Outdoor. The received power is negatively correlated with both τ and τ_{rms}. In general, the correlation tends to increase with the size of the environment, with the outdoor case being highly correlated. The model is able to replicate the varying correlation between P_0 and τ_{rms} that is observed in the data, as opposed to having a fixed correlation coefficient suggested in [11]. Note that the correlation coefficient between $\bar{\tau}$ and τ_{rms} for the model fitted to the Lille data set is not within the bootstrap interval. This is due to the banana-like shape of their scatter plot which is not replicated by the model (see Fig. 7).

VIII. CONCLUSION

Joint modeling of received power, mean delay, and rms delay spread provides more accurate models in a range of scenarios as opposed to independent modeling. The proposed model of the multivariate log-normal distribution seems to be a reasonable choice for simulating these standardized moments, however, the fit can be improved by using more complex models. The proposed model is simple, easy to simulate from, and easy to fit to new measurements in both indoor and outdoor settings using standard estimators. The raw temporal moments are dependent random variables which should be simulated jointly; as a result, the same is also true for the standardized temporal moments. The correlation of these moments changes from scenario to scenario, but can be inferred efficiently in each case.

In the light of the strong correlation observed in the measurements, assuming independence might lead to significant errors in some applications. Hence, reporting of the marginal distributions of the standardized moments is insufficient and a clearer picture can be obtained by considering both their means and covariances. The correlation between these standardized moments can be used to validate multipath models instead of just their marginal fits. The correlation should also be accounted for in the analysis and simulation of radio channels.

The means and covariances of the temporal moments potentially depend on a number of physical factors. The relationship between the means and the transmitter-receiver distance has been studied for indoor scenarios. However, the effect of the distance on the covariance matrix is presently unclear. For multipath models, the covariance matrix is known to depend on the first- and second-order intensity functions which governs the arrival process. Since both intensity functions are affected by antenna directivity, the covariance matrix should also be. Nevertheless, these effects are not yet well-understood and should be the topic of further studies.

ACKNOWLEDGMENT

The authors would like to thank Dr. Carl Gustafson and Prof. Fredrik Tufvesson (Lund University) for providing the measurement data.

APPENDIX
PARAMETER INFERENCE FOR THE LOG-NORMAL

In this section, we recall how to derive the maximum likelihood estimates and related confidence intervals for a log-normal distribution. Let $Y = (Y_1, \ldots, Y_d)$ be a multivariate log-normal random variable. We will denote this distribution $\mathcal{LN}(\boldsymbol{\mu}, \boldsymbol{\Sigma})$, where $\boldsymbol{\mu}$ and $\boldsymbol{\Sigma}$ denote the parameters. Then, $X = (X_1, \ldots, X_d) = (\log(Y_1), \ldots, \log(Y_d))$ is a multivariate Gaussian random variable with mean vector $\boldsymbol{\mu}$ and covariance matrix $\boldsymbol{\Sigma}$. ta, wSince the maximum likelihood estimator is invariant to one-to-one transformations of the dae can simply take the logarithm of our data points and compute the maximum likelihood estimate corresponding to Gaussian data. Given N i.i.d. observations $\{\mathbf{y}_i\}_{i=1}^N$, we hence compute $\mathbf{x}_i = \log \mathbf{y}_i$ for $i = 1, \ldots, N$, and return the following estimates:

$$\hat{\boldsymbol{\mu}} = \frac{1}{N}\sum_{i=1}^{N} \mathbf{x}_i, \quad \text{and} \tag{13}$$

$$\hat{\boldsymbol{\Sigma}} = \frac{1}{N}\sum_{i=1}^{N} (\mathbf{x}_i - \hat{\boldsymbol{\mu}})(\mathbf{x}_i - \hat{\boldsymbol{\mu}})^\top. \tag{14}$$

Now, let the K free parameters be combined into a single vector $\boldsymbol{\theta} = (\boldsymbol{\alpha}, \boldsymbol{\beta})$, where $\boldsymbol{\alpha} = (\mu_1, \ldots, \mu_d)$, and $\boldsymbol{\beta} = (\Sigma_{11}, \ldots, \Sigma_{dd})$. Note that $\Sigma_{ij} = \Sigma_{ji}$. The Fisher information matrix reads

$$I(\boldsymbol{\alpha}, \boldsymbol{\beta}) = \begin{bmatrix} I(\boldsymbol{\alpha}) & \mathbf{0} \\ \mathbf{0} & I(\boldsymbol{\beta}) \end{bmatrix} \tag{15}$$

where, for $1 \leq m, n \leq K$, the (m, n) entry of the matrix is

$$I(\boldsymbol{\alpha})_{m,n} = \frac{\partial \boldsymbol{\mu}^{\top}}{\partial \alpha_m} \boldsymbol{\Sigma}^{-1} \frac{\partial \boldsymbol{\mu}}{\partial \alpha_n}, \quad 1 \leq m, n \leq d \tag{16}$$

$$I(\boldsymbol{\beta})_{m,n} = \frac{1}{2} \mathrm{tr}\left(\boldsymbol{\Sigma}^{-1} \frac{\partial \boldsymbol{\Sigma}}{\partial \beta_m} \boldsymbol{\Sigma}^{-1} \frac{\partial \boldsymbol{\Sigma}}{\partial \beta_n} \right). \tag{17}$$

On further simplification, the entries of the Fisher information matrix become

$$I(\boldsymbol{\alpha})_{m,n} = \boldsymbol{\Sigma}^{-1}_{mn}, \tag{18}$$

$$I(\boldsymbol{\beta})_{m,n} = \frac{1}{2} \mathrm{tr}\left(\boldsymbol{\Sigma}^{-1} \mathbf{E}_m \boldsymbol{\Sigma}^{-1} \mathbf{E}_n \right) \tag{19}$$

where $\mathbf{E}_m$ is a $d \times d$ matrix of all zeros except the (i, i) entry corresponding to $\boldsymbol{\beta}_m = \Sigma_{ii}$ which is 1. Note that for $\boldsymbol{\beta}_m = \Sigma_{ij}, i \neq j$, both (i, j) and (j, i) entry of $\mathbf{E}_m$ will be 1. Same goes for $\mathbf{E}_n$. The 95% confidence interval for the mth parameter of the Gaussian, $(\theta_m \pm \delta_m)$ is

$$\theta_m \pm \frac{1.96}{\sqrt{N}} \sqrt{\mathbf{I}^{-1}_{m,m}}$$

where $\mathbf{I}^{-1}_{m,m}$ is the (m, m) entry of $\mathbf{I}^{-1}$.

REFERENCES

[1] A. Goldsmith, *Wireless Communications*. Cambridge, U.K.: Cambridge Univ. Press, Aug. 2005.

[2] W.-D. Wu, C.-H. Wang, C.-C. Chao, and K. Witrisal, "On parameter estimation for ultra-wideband channels with clustering phenomenon," in *Proc. IEEE 68th Veh. Technol. Conf.*, Sep. 2008, pp. 1–5.

[3] A. Bharti, R. Adeogun, and T. Pedersen, "Parameter estimation for stochastic channel models using temporal moments," in *Proc. IEEE Int. Symp. Antennas Propag. USNC-URSI Radio Sci. Meeting*, Jul. 2019, pp. 1267–1268.

[4] A. Bharti, R. Adeogun, and T. Pedersen, "Estimator for stochastic channel model without multipath extraction using temporal moments," in *Proc. IEEE 20th Int. Workshop Signal Process. Adv. Wireless Commun. (SPAWC)*, Jul. 2019, pp. 1–5.

[5] A. Bharti and T. Pedersen, "Calibration of stochastic channel models using approximate Bayesian computation," in *Proc. IEEE Globecom Workshops (GC Wkshps)*, Dec. 2019, pp. 1–6.

[6] A. Bharti, R. Adeogun, and T. Pedersen, "Learning parameters of stochastic radio channel models from summaries," *IEEE Open J. Antennas Propag.*, vol. 1, pp. 175–188, 2020.

[7] R. Adeogun, "Calibration of stochastic radio propagation models using machine learning," *IEEE Antennas Wireless Propag. Lett.*, vol. 18, no. 12, pp. 2538–2542, Dec. 2019.

[8] Z. Latinovic and H. Huang, "A channel model for indoor time-of-arrival ranging," *IEEE Trans. Wireless Commun.*, vol. 19, no. 2, pp. 1415–1428, Feb. 2020.

[9] M. K. Awad, K. T. Wong, and Z.-b. Li, "An integrated overview of the open Literature's empirical data on the indoor radiowave channel's delay properties," *IEEE Trans. Antennas Propag.*, vol. 56, no. 5, pp. 1451–1468, May 2008.

[10] D. Cox and R. Leck, "Distributions of multipath delay spread and average excess delay for 910-MHz urban mobile radio paths," *IEEE Trans. Antennas Propag.*, vol. AP-23, no. 2, pp. 206–213, Mar. 1975.

[11] L. J. Greenstein, V. Erceg, Y. S. Yeh, and M. V. Clark, "A new path-gain/delay-spread propagation model for digital cellular channels," *IEEE Trans. Veh. Technol.*, vol. 46, no. 2, pp. 477–485, May 1997.

[12] J. Fischer, M. Grossmann, W. Felber, M. Landmann, and A. Heuberger, "A novel delay spread distribution model for VHF and UHF mobile-to-mobile channels," in *Proc. 7th Eur. Conf. Antennas Propag., EuCAP*, Apr. 2013, pp. 469–472.

[13] G. Wang, G. Zhu, S. Lin, J. Ding, D. Fei, and H. Zhang, "Channel measurement and modeling in highway scenario at 460 MHz," in *Proc. IEEE Int. Symp. Antennas Propag. USNC-URSI Radio Sci. Meeting*, Jul. 2019, pp. 2119–2120.

[14] J. Li, B. Ai, R. He, M. Yang, and Z. Zhong, "Multi-frequency channel characterization for massive MIMO communications in lobby environment," *China Commun.*, vol. 16, no. 9, pp. 79–92, Sep. 2019.

[15] X. Zhang, G. Qiu, J. Zhang, L. Tian, P. Tang, and T. Jiang, "Analysis of millimeter-wave channel characteristics based on channel measurements in indoor environments at 39 GHz," in *Proc. 11th Int. Conf. Wireless Commun. Signal Process. (WCSP)*, Oct. 2019, pp. 1–6.

[16] Y. Yu, Y. Liu, W. Lu, and H. Zhu, "Measurement and empirical modelling of root mean square delay spread in indoor femtocells scenarios," *IET Commun.*, vol. 11, no. 13, pp. 2125–2131, Sep. 2017.

[17] M. Schmieder, T. Eichler, S. Wittig, M. Peter, and W. Keusgen, "Measurement and characterization of an indoor industrial environment at 3.7 and 28 GHz," in *Proc. 14th Eur. Conf. Antennas Propag. (EuCAP)*, Mar. 2020, pp. 1–5.

[18] J. Yu *et al.*, "Channel measurement and modeling of the small-scale fading characteristics for urban inland river environment," *IEEE Trans. Wireless Commun.*, vol. 19, no. 5, pp. 3376–3389, May 2020.

[19] Y. Yu, W.-J. Lu, Y. Liu, and H.-B. Zhu, "Neural-network-based root mean delay spread model for ubiquitous indoor Internet-of-Things scenarios," *IEEE Internet Things J.*, vol. 7, no. 6, pp. 5580–5589, Jun. 2020.

[20] A. Prokes, T. Mikulasek, M. Waldecker, B. K. Engiz, and J. Blumenstein, "Multipath propagation analysis for static urban environment at 60 GHz," in *Proc. Int. Conf. Electr. Comput. Technol. Appl. (ICECTA)*, Nov. 2019, pp. 1–4.

[21] M. S. Varela and M. G. Sanchez, "RMS delay and coherence bandwidth measurements in indoor radio channels in the UHF band," *IEEE Trans. Veh. Technol.*, vol. 50, no. 2, pp. 515–525, Mar. 2001.

[22] G. Steinbock, T. Pedersen, B. H. Fleury, W. Wang, and R. Raulefs, "Distance dependent model for the delay power spectrum of in-room radio channels," *IEEE Trans. Antennas Propag.*, vol. 61, no. 8, pp. 4327–4340, Aug. 2013.

[23] T. Pedersen, "Modeling of path arrival rate for in-room radio channels with directive antennas," *IEEE Trans. Antennas Propag.*, vol. 66, no. 9, pp. 4791–4805, Sep. 2018.

[24] T. Pedersen, "Stochastic multipath model for the in-room radio channel based on room electromagnetics," *IEEE Trans. Antennas Propag.*, vol. 67, no. 4, pp. 2591–2603, Apr. 2019.

[25] S. Kotz, N. Balakrishnan, and N. L. Johnson, *Continuous Multivariate Distributions*. Hoboken, NJ, USA: Wiley, Apr. 2000.

[26] R. B. Nelsen, *An Introduction to Copulas*. Berlin, Germany: Springer-Verlag, 2007. [Online]. Available: https://www.ebook.de/de/product/5270140/roger_b_nelsen_an_introduction_%to_copulas.html

[27] C. Gustafson, D. Bolin, and F. Tufvesson, "Modeling the polarimetric mm-wave propagation channel using censored measurements," in *Proc. IEEE Global Commun. Conf. (GLOBECOM)*, Dec. 2016, pp. 1–6.

[28] M. Fryziel, C. Loyez, L. Clavier, N. Rolland, and P. A. Rolland, "Path-loss model of the 60-GHz indoor radio channel," *Microw. Opt. Technol. Lett.*, vol. 34, no. 3, pp. 158–162, Aug. 2002. [Online]. Available: https://onlinelibrary.wiley.com/doi/abs/10.1002/mop.10402

[29] M. Razzaghpour *et al.*, "Short-range UWB wireless channel measurement in industrial environments," in *Proc. Int. Conf. Wireless Mobile Comput., Netw. Commun. (WiMob)*, Oct. 2019, pp. 1–6.

[30] A. Bharti, L. Clavier, and T. Pedersen, "Joint statistical modeling of received power, mean delay, and delay spread for indoor wideband radio channels," in *Proc. 14th Eur. Conf. Antennas Propag. (EuCAP)*, Mar. 2020, pp. 1–5.

[31] A. W. Mbugua, W. Fan, K. Olesen, X. Cai, and G. F. Pedersen, "Phase-compensated optical fiber-based ultrawideband channel sounder," *IEEE Trans. Microw. Theory Techn.*, vol. 68, no. 2, pp. 636–647, Feb. 2020.

[32] X. Cai and W. Fan, "A complexity-efficient high resolution propagation parameter estimation algorithm for ultra-wideband large-scale uniform circular array," *IEEE Trans. Commun.*, vol. 67, no. 8, pp. 5862–5874, Aug. 2019.

[33] H. Akaike, "A new look at the statistical model identification," *IEEE Trans. Autom. Control*, vol. 19, no. 6, pp. 716–723, Dec. 1974.

[34] G. Claeskens and N. L. Hjort, *Model Selection Model Averaging*. Cambridge, U.K.: Cambridge Univ. Press, 2008.

[35] J. Ding, V. Tarokh, and Y. Yang, "Model selection techniques: An overview," *IEEE Signal Process. Mag.*, vol. 35, no. 6, pp. 16–34, Nov. 2018.

[36] J. A. Rice, *Mathematical Statistics and Data Analysis*, 2nd ed. Pacific Grove, CA, USA: Duxbury Press, 1994.

[37] B. Efron and R. Tibshirani, *An Introduction to Bootstrap*. London, U.K.: Chapman & Hall, May 1994.

Ayush Bharti (Member, IEEE) received the B.E. degree in electrical and electronics engineering from the Birla Institute of Technology and Sciences, Pilani, India, in 2015, and the M.Sc. degree in signal processing and computing from Aalborg University, Aalborg, Denmark, in 2017, where he is currently pursuing the Ph.D. degree with the Department of Electronic Systems.

His research interests include likelihood-free inference, statistical signal processing, and radio channel modeling.

Ramoni Adeogun (Senior Member, IEEE) received the B.Eng. degree in electrical and computer engineering from the Federal University of Technology, Minna, Nigeria, in 2007, and the Ph.D. degree in electronic and computer systems engineering from the Victoria University of Wellington, Wellington, New Zealand, in 2015.

He is currently a Post-Doctoral Fellow at Aalborg University, Aalborg, Denmark, and also as an External Research Engineer with Nokia Bell Labs, Aalborg. Prior to joining Aalborg University, he has also worked in various positions at the University of Cape Town, SA, Odua Telecoms Ltd., and the National Space Research and Development Agency, Nigeria. His research interests include channel characterization, machine learning and AI for communications, intelligent spectrum access, and interference management.

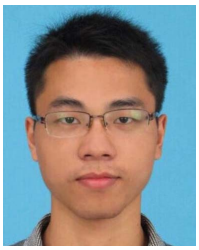

Xuesong Cai received the B.S. and Ph.D. degrees (Hons.) from Tongji University, Shanghai, China, in 2013 and 2018, respectively.

In 2015, he conducted a three-month internship with Huawei Technologies, Shanghai. He was also a Visiting Scholar with the Universidad Politécnica de Madrid, Madrid, Spain, in 2016. From 2018 to 2020, he was a Post-Doctoral Research Fellow with the APMS Section, Department of Electronic Systems, Aalborg University (AAU), Aalborg, Denmark. Since April 2020, he has been a Post-Doctoral Fellow with the Wireless Communication Networks Section, Department of Electronic Systems, AAU, cooperating with Nokia Bell Labs. His research interests include propagation channel measurement, high-resolution parameter estimation, channel characterization, channel modeling, over-the-air testing, and UAV communications for 5G wireless communications.

Dr. Cai was a recipient of the Chinese National Scholarship for Ph.D. Candidates and the Excellent Student Award in 2016, the Excellent Student Award and the "ZTE Fantastic Algorithm" Award in 2017, the Outstanding Doctorate Graduate awarded by the Shanghai Municipal Education Commission and "ZTE Blue Sword-Future Leaders Plan" in 2018, and the "Seal of Excellence" with the European Horizon 2020's Marie Skłodowska-Curie actions call in 2019.

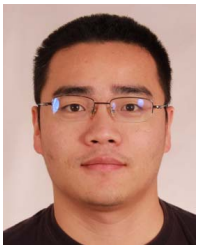

Wei Fan (Senior Member, IEEE) received the Bachelor of Engineering degree from the Harbin Institute of Technology, Harbin, China, in 2009, the master's double degree (Hons.) from the Politecnico di Torino, Turin, Italy, and the Grenoble Institute of Technology, Grenoble, France, in 2011, and the Ph.D. degree from Aalborg University, Aalborg, Denmark, in 2014.

From February 2011 to August 2011, he was with Intel Mobile Communications, Herlev, Denmark, as a Research Intern. He conducted a three-month internship at Anite Telecoms OY, Oulu, Finland, in 2014. He is now an Associate Professor with Aalborg University. His main areas of research are over-the-air testing of multiple antenna systems, radio channel sounding, modeling, and emulation.

François-Xavier Briol received the bachelor's degree with integrated master's degree in mathematics, operational research, statistics and economics (MMORSE) and the Ph.D. degree in statistics from the University of Warwick, Coventry, U.K., in 2014 and 2019, respectively.

He was briefly a Research Associate at Imperial College London, London, U.K., and the University of Cambridge, Cambridge, U.K., before joining University College London (UCL) in 2019, where he is now a Lecturer in statistical science. He is also a Group Leader in data-centric engineering at The Alan Turing Institute, the U.K.'s national institute for data science and AI, where he currently leads a project on "Fundamentals of Statistical Machine Learning." His research interests include statistical computation and inference for large-scale and computationally expensive probabilistic models.

Laurent Clavier (Senior Member, IEEE) received the Ph.D. degree in signal processing from TELECOM Bretagne (now IMT Atlantique), Brest, France, in 1997, and the HDR degree from Lille University, Lille, France, in 2009.

Since October 2011, he has been a Professor with the Mines-Telecom Institute (IMT Lille Douai), the Institut d'Electronique de Microélectronique et de Nanotechnolo-gie (IEMN) (UMR CNRS 8520), and the Institut de Recherche sur les composants logiciels et matériels pour l'Information et la Communication Avancée (IRCICA) (USR CNRS 3380). His research activities concern digital communications and the physical layer of wireless networks for the IoT, more specifically energy autonomous sensor networks. He is particularly interested in the interference model and impact on ultradense wireless networks.

Troels Pedersen (Member, IEEE) received the M.Sc. degree in digital communications and the Ph.D. degree in wireless communications from Aalborg University, Aalborg, Denmark, in 2004 and 2009, respectively.

In 2005, he was a Guest Researcher with the FTW Telecommunications Research Center Vienna, Vienna, Austria. He joined the Department of Electronic Systems, Aalborg University, as an Assistant Professor, in 2009, and became an Associate Professor in 2012. In 2012, he was a Visiting Professor with the Institut d'Électronique et de Télécommunications de Rennes, University of Rennes 1, Rennes, France. His current research interests include statistical signal processing and communication theory, including sensor array signal processing, radio geolocation techniques, radio channel modeling, and radio channel sounding.

Dr. Pedersen received the Teacher of the Year Award from the Study Board for Electronics and IT, Aalborg University, in 2011 and 2017.